JOURNAL OF GUIDANCE, CONTROL, AND DYNAMICS
Vol. 31, No. 4, July–August 2008

Imaging Sensors Pointing and Tracking Controller Insensitive to Inertial Sensors Misalignments

Hari B. Hablani*
The Boeing Company, Huntington Beach, California 92647-2099

DOI: 10.2514/1.33014

This paper is concerned with a pointing controller for an imaging sensor mounted on a chaser satellite to track a target satellite to rendezvous. Inertial attitude of the imaging sensor is estimated with gyros and star trackers and a Kalman filter. It is shown that the pointing accuracy of the imaging sensor is independent of the misalignments of the gyros and star tracker axes with the imaging sensor axes. This is important because the misalignments may be uncalibrated or unknown. This paper presents the pointing controller, its analysis, and simulation results that support the claim. Further, the results demonstrate that the controller meets the pointing accuracy requirement under various misalignment conditions between the imaging sensor and the gyros and star trackers.

I. Introduction

THIS paper is concerned with 1) the design of a pointing and tracking controller for an imaging sensor mounted on a chaser satellite, aided by misaligned gyros and star trackers, and 2) the evaluation of the controller's pointing accuracy while tracking a client satellite for rendezvous.

The paper is organized as follows. Section II presents the imaging sensor pointing and tracking controller and analysis of its pointing accuracy. Briefly, the pointing and tracking system comprises an imaging sensor, misaligned gyros and a star tracker for inertial attitude estimation of the focal plane with a Kalman filter, an extended Kalman filter for inertial relative navigation of the target satellite, glide-slope guidance for rendezvous, pointing and rate commands for tracking a target satellite, and an attitude controller. No alignment Kalman filter is used to calibrate the gyros and the star tracker. Therefore, when an attitude estimator receives measurements from the gyros and star tracker that are misaligned with the spacecraft axes or optic axes, the attitude estimation errors develop nonzero means. These mean errors cause errors in relative navigation of the target satellite, which in turn cause errors in the attitude and rate commands for pointing and tracking the target satellite. Transfer functions are developed that relate focal plane image angles with the attitude and rate command estimation errors and attitude and rate estimation errors. A linear statistical analysis is applied to evaluate the focal plane image angle caused by these estimation errors. The means of the attitude estimation errors and their variances are formulated in Sec. III. Expressions of steady-state pre- and postupdate mean attitude estimation errors with star tracker measurements are developed, and how attitude estimation errors affect relative navigation of the target satellite is shown. Section IV summarizes quaternion pointing commands and rate commands for tracking a target satellite. Section V presents simulation results for a rendezvous scenario that calls upon all of the above components of pointing and tracking and glide-slope guidance. Attitude estimation errors and line-of-sight (LOS) command estimation errors due to the gyros and star tracker misalignments are illustrated. It is then shown that the attitude error signal inputted to the attitude controller is independent of these misalignments, however, and apart from high-frequency noise the attitude error signal is nearly the same as the focal plane image angle, as intuition might suggest. The focal plane pointing accuracy is shown to be unaffected by the misalignments, and the pointing accuracy requirement is shown to be met just the same whether gyros and star trackers are misaligned with the optical bench or not. Section VI concludes the paper.

Presented as Paper 2005-5982 at the AIAA Guidance, Navigation, and Control Conference, Austin, Texas, August 2005; received 22 June 2007; revision received 15 September 2007; accepted for publication 16 September 2007.

*Technical Fellow, Flight Sciences and Advanced Design. Associate Fellow AIAA.

II. Pointing Error Analysis of an Optical Navigation System

Figure 1 portrays a single-axis closed-loop control system for pointing an imaging sensor at a target satellite and tracking it. An early multi-axis version of this controller is presented in [1], but our objective here is to relate the focal plane angle of the target image with various error sources in the tracking system—a task analyzable more clearly in a single-axis setup. Intuitively, because the aim of the control system is to point the focal plane boresight at the target, it is the focal plane image angle ε that is to be nulled and is of central importance; the spacecraft attitude control enables this process, but the spacecraft attitude and rate are quite possibly internal variables and should not be involved in the evaluation of the pointing accuracy. This thought will be our guide in the following pointing analysis. A single-axis (spacecraft y-axis) dynamics is considered below.

A. Focal Plane Image Angle and Its Estimate

As the inset diagram in Fig. 1 indicates, in the absence of any errors or measurement noise, the focal plane angle ε is related to the focal plane boresight attitude θ_y and the commanded pointing angle θ_{yc}, both measured from the same inertial reference, as

$$\varepsilon = \theta_{yc} - \theta_y \tag{1}$$

This equation or its equivalent form $\theta_{yc} = \theta_y + \varepsilon$ is valid whether the image angle ε has a zero mean or nonzero. Further, Eq. (1) reveals that the usual attitude error signal $(\theta_{yc} - \theta_y)$ fed to a compensator would be the same as the focal plane angle ε if both θ_{yc} and θ_y were known. However, neither is known exactly; the angle θ_{yc} is estimated from an estimate of the relative position of the target satellite from the chaser satellite, denoted $\hat{\boldsymbol{\ell}}$, and the spacecraft attitude θ_y is measured with gyros and star trackers and is estimated with an attitude determination Kalman filter (Fig. 1). These angle estimates, denoted $\hat{\theta}_{yc}$ and $\hat{\theta}_y$, respectively, have estimation errors, usually denoted as $\tilde{\theta}_{yc}$ and $\tilde{\theta}_y$, defined by $\hat{\theta}_{yc} = \theta_{yc} + \tilde{\theta}_{yc}$, and $\hat{\theta}_y = \theta_y + \tilde{\theta}_y$. The pointing command error $\tilde{\theta}_{yc}$ is due to the error in the relative position estimate $\hat{\boldsymbol{\ell}}$ which, along with the relative velocity estimate $\hat{\dot{\boldsymbol{\ell}}}$ needed to determine the rate command, is output of a relative navigation Kalman filter [2]. As portrayed in Fig. 1, this Kalman filter uses focal plane measurements, inertial attitude estimates, accelerometer

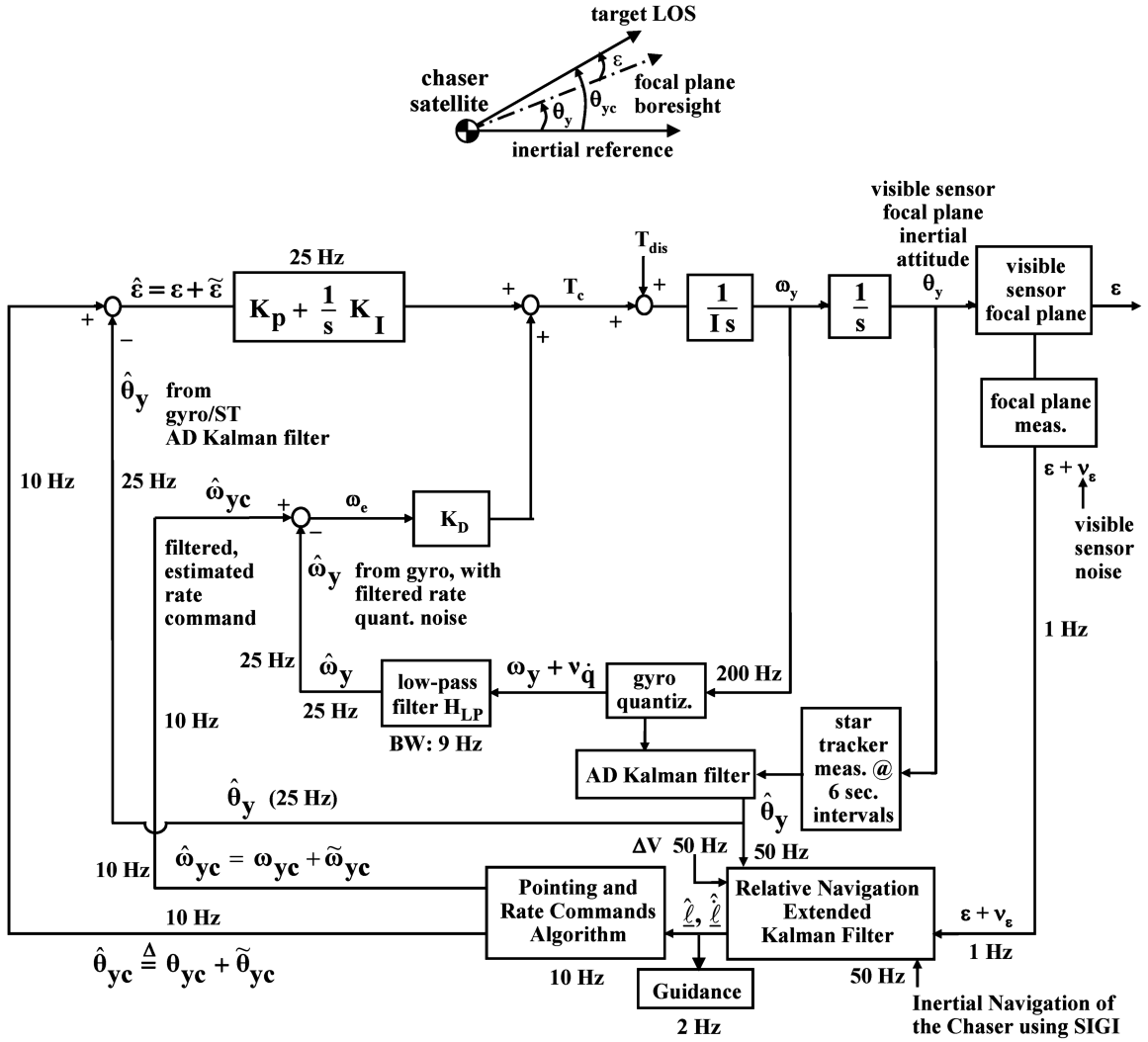

Fig. 1 Single-axis closed-loop focal plane pointing and tracking.

measurements of the incremental velocity ΔV for guidance, and inertial position and velocity estimates of the own spacecraft furnished by an inertial navigation system (SIGI, Space Integrated GPS INS). As a result, the error $\tilde{\theta}_{yc}$ depends on the errors in these inputs and also on the noise attenuation property of the relative navigation Kalman filter. As shown in Fig. 1, the attitude control error signal $\hat{\varepsilon}$, which is indeed an estimate of the focal plane image angle ε, fed to the compensator is equal to

$$\hat{\varepsilon} = \hat{\theta}_{yc} - \hat{\theta}_y = \varepsilon + \tilde{\theta}_{yc} - \tilde{\theta}_y = \varepsilon + \tilde{\varepsilon} \tag{2}$$

The error in this estimate is thus equal to $\tilde{\varepsilon} \triangleq \tilde{\theta}_{yc} - \tilde{\theta}_y$ and consists of both the attitude command estimation error and attitude determination error. Note that the attitude error signal $\hat{\varepsilon}$ is actually independent of the spacecraft attitude, as expected.

B. Rate Error and Its Estimate

Besides the error signal $\hat{\varepsilon}$, the compensator requires a rate error also to damp $\hat{\varepsilon}$. Ideally, the rate error is defined as $\omega_e = \omega_{yc} - \omega_y$ where ω_{yc} and ω_y are the inertial rate command and the inertial rate, respectively. But only the estimates of these variables are known. While the inertial rate command ω_{yc} is estimated from the estimates of the relative position and velocity of the target from the spacecraft, $\hat{\boldsymbol{\ell}}$ and $\hat{\dot{\boldsymbol{\ell}}}$, the spacecraft rate ω_y is measured by a gyro which, due to quantization of the measured incremental angle over, say, 5 ms, causes a quantization rate noise $\nu_{\dot{q}}$ (Fig. 1). The gyro-measured rate is therefore equal to $(\omega_y + \nu_{\dot{q}})$. In the application that sponsored this work, the quantization rate noise $\nu_{\dot{q}}$ was far greater than the gyro drift rate. Further, the gyro drift rate is estimated by the attitude estimator, subtracted from the measurements, and corrected periodically with the star track measurements. Therefore, the gryro rate is not included in the analysis in this section, but is considered in Sec. III. Because the quantization rate noise is usually significant, the gyro measurement is passed through a first-order low-pass filter $H_{\mathrm{LP}} = \omega_{\mathrm{LP}}/(s + \omega_{\mathrm{LP}}) = 1/(1 + \tau_{\mathrm{LP}} s)$ where ω_{LP} is the bandwidth of the filter and $\tau_{\mathrm{LP}} = 1/\omega_{\mathrm{LP}}$ its time constant. The rate estimate $\hat{\omega}_y$, the output of this filter, is $\hat{\omega}_y = H_{\mathrm{LP}}(\omega_y + \nu_{\dot{q}})$. The rate error signal ω_e is then (Fig. 1)

$$\omega_e = \hat{\omega}_{yc} - H_{\mathrm{LP}}(\omega_y + \nu_{\dot{q}}) \tag{3}$$

Analogous to the attitude error signal $\hat{\varepsilon}$, which is independent of the spacecraft attitude, it is useful to express ω_e also independent of the spacecraft rate. For this purpose, observe that the rate command estimation error $\tilde{\omega}_{yc}$ is usually defined as $\hat{\omega}_{yc} = \omega_{yc} + \tilde{\omega}_{yc}$. To eliminate the spacecraft rate ω_y $(=\dot{\theta}_y)$ from ω_e, differentiate Eq. (1), yielding

$$\dot{\varepsilon} = \dot{\theta}_{yc} - \dot{\theta}_y \triangleq \omega_{yc} - \omega_y \tag{4}$$

substitute $\hat{\omega}_{yc} = \omega_{yc} + \tilde{\omega}_{yc}$ and $\omega_y = \omega_{yc} - \dot{\varepsilon}$ from Eq. (4) in Eq. (3), and arrive at

$$\omega_e = (1 - H_{\mathrm{LP}})\omega_{yc} + \tilde{\omega}_{yc} + H_{\mathrm{LP}}(\dot{\varepsilon} - \nu_{\dot{q}}) \tag{5}$$

which is now independent of the spacecraft attitude and rate. As a side comment, note that this equation suggests that to minimize the rate error, the low-pass filter bandwidth should be higher than the

bandwidth of the rate command ω_{yc}, the rate command estimation error $\tilde{\omega}_{yc}$ should be small, and the low-pass filter bandwidth should be no higher than necessary so as to minimize its response to the wideband quantization rate noise $\nu_{\dot{q}}$.

C. Transfer Function of the Focal Plane Image Angle

To determine pointing accuracy ε of the controller, that is, the focal plane image angle, it is now related with the pointing commands, disturbance acceleration $\alpha_d(t)$, and various error sources introduced above. In particular, we derive the following transfer function between $\varepsilon(s)$ and the variables just mentioned

$$\varepsilon(s) = \frac{1}{p'(s)}\left[\theta_{yc} - \frac{1}{s^2}\omega_{yc}(1 - H_{\mathrm{LP}})a_d\right] - \frac{1}{s^2 p'(s)}\alpha_d(s) - \frac{1}{s^2 p'(s)}\left[\tilde{\varepsilon}\left(a_p + \frac{1}{s}a_I\right) + (\tilde{\omega}_{yc} - H_{\mathrm{LP}}\nu_{\dot{q}})a_d\right] \tag{6}$$

where the polynomial $p'(s)$ is

$$p'(s) = \frac{1}{s^3}[s^3 + H_{\mathrm{LP}}a_d s^2 + a_p s + a_I] \tag{7}$$

and the proportional, integral, and derivative (PID) gains are defined as $a_p = K_P/I$, $a_d = K_D/I$, and $a_I = K_I/I$, with I as the moment of inertia of the spacecraft about the axis in consideration; α_d is the disturbance acceleration. In deriving the above transfer function, the focal plane image rate $\dot{\varepsilon}$ is expressed as $s\,\varepsilon\,(s)$, θ_y is substituted in terms of ε and θ_{yc}, and likewise the rate $\dot{\theta}_y = \omega_y$ is replaced in terms of $\dot{\varepsilon}$ and ω_{yc}. The numerator of the polynomial $p'(s)$ above appears as cubic, but because H_{LP} is a first-order filter, the $p'(s)$ becomes quartic on simplification. However, because the bandwidth of H_{LP} must be much higher than the bandwidth of the PID controller, $H_{\mathrm{LP}} = 1$ within the controller bandwidth and the numerator of $p'(s)$ is essentially cubic. Also, inasmuch as the PID controller bandwidth is intended to be much higher than the bandwidths of the pointing command θ_{yc}, rate command ω_{yc}, and disturbance acceleration α_d, most of the pointing error is caused by the pointing command and rate command estimation errors $\tilde{\theta}_{yc}$ and $\tilde{\omega}_{yc}$, and the attitude and rate determination errors $\tilde{\theta}_y$ and $\nu_{\dot{q}}$. As such, we will focus on these error sources next.

Recall that the estimation error $\tilde{\varepsilon}$ in Eq. (6) equals $\tilde{\theta}_{yc} - \tilde{\theta}_y$. The error $\tilde{\theta}_{yc}$ arises from the relative position estimation error $\tilde{\boldsymbol{\ell}}$. One of the sources of $\tilde{\boldsymbol{\ell}}$ is the attitude estimation error $\tilde{\theta}_y$ because $\hat{\theta}_y$ is fed to the relative navigation extended Kalman filter (Fig. 1). If the error $\tilde{\theta}_y$ has a nonzero mean due to the gyro and star tracker misalignments, this mean error (time varying as we shall see in Sec. III) will misalign the inertial frame in which $\boldsymbol{\ell}$ and $\dot{\boldsymbol{\ell}}$ are estimated, and then manifest itself in $\tilde{\theta}_{yc}$. A statistical analysis of attitude estimation error due to the misalignment angles is developed in Sec. III. Meanwhile we note that the misalignment angles apparently null themselves from $\tilde{\theta}_{yc} - \tilde{\theta}_y$. There may still be some bias error in the estimates $\hat{\boldsymbol{\ell}}$ and $\hat{\dot{\boldsymbol{\ell}}}$ due to other sources of errors in the inputs to the relative navigation filter—inertial navigation, for instance, or due to the filter's inherent linear approximation. Denote the mean error signal as $\bar{\tilde{\varepsilon}} = \bar{\tilde{\theta}}_{yc} - \bar{\tilde{\theta}}_y$, where $(\bar{\cdot})$ is the mean of the estimation error $(\tilde{\cdot})$. One can show with the aid of the final value theorem that, due to the integral gain in the attitude controller, the steady-state pointing accuracy ε is $\varepsilon = \bar{\tilde{\varepsilon}}$.

D. Standard Deviation of the Focal Plane Image Angle

We will first determine the image angle ε due to the zero-mean random error component in $\tilde{\varepsilon}$ caused by the attitude estimation error $\tilde{\theta}_y$. The variance of $\tilde{\theta}_y$ depends on the gyro and star tracker random errors and star tracker measurement update interval, as analyzed in [2,3]. The zero-mean random error in $\tilde{\varepsilon}$ due to $\tilde{\theta}_{yc}$ may be significant also due to the errors in the inertial navigation of the chaser satellite, depending on the noise attenuation properties [4] of the relative navigation extended Kalman filter. However, regarding the image angle ε due to $\tilde{\theta}_y$, note the following transfer function between ε and the estimation error $\tilde{\theta}_y(s)$ from Eq. (6):

$$\varepsilon(s) = \frac{1}{s^2 p'(s)}(a_p + a_I/s)\tilde{\theta}_y(s) \tag{8}$$

which agrees with Eq. (3) of [5]. Denoting the standard deviation (s.d.) of the attitude estimation error as $\sigma_{\tilde{\theta}}$, we note that, in steady state, it is maximum before the star tracker measurement update and minimum after the update [3]. Assuming that the maximum value prevails all the time, standard deviation σ_ε of the pointing accuracy ε in Eq. (8) due to $\sigma_{\tilde{\theta}}$ with the PID attitude controller operating at a sampling frequency f_s will be, by applying the linear statistical analysis [6,7],

$$\sigma_\varepsilon^2 = \frac{\sigma_{\tilde{\theta}}^2}{2f_s}\frac{a_p^2 + a_d a_I}{a_d a_p - a_I} \tag{9}$$

assuming that $H_{\mathrm{LP}} = 1$ in the characteristic equation (7).

Regarding the rate error $\tilde{\omega}_{yc} - H_{\mathrm{LP}}\nu_{\dot{q}}$ in Eq. (6), we again assume that the rate command estimation error $\tilde{\omega}_{yc}$ is not significant compared to the filtered rate quantization noise $H_{\mathrm{LP}}\nu_{\dot{q}}$ and therefore we focus on the image angle ε caused by this rate noise only. Note that H_{LP} cannot be treated as unity now because the purpose of H_{LP} is to attenuate $\nu_{\dot{q}}$ noise. For statistical error analysis, variance of the rate quantization noise is required. Franklin et al. in [8] shows that if the spacecraft attitude θ_y is quantized with q rad per pulse, the quantization error can be approximated then as a band-limited white noise with the standard deviation $\sigma_q = q/\sqrt{12}$. If f_s is the output sample frequency of the gyro (200 Hz in Fig. 1), then the flat spectrum of the quantization error is limited to $-0.5f_s \le f \le 0.5f_s$, and standard deviation $\sigma_{\dot{q}}$ of the rate noise is [9] $\sigma_{\dot{q}} = \sqrt{2}\sigma_q/\tau_s$, where τ_s is the sample period of the gyro output, equal to $1/f_s$. The corresponding power spectral density of the band-limited rate noise $\nu_{\dot{q}}$ is $V_{\dot{q}} = \sigma_{\dot{q}}^2/f_s$. Variance of the pointing error is then found to be [6,7]

$$\sigma_\varepsilon^2 = \frac{a_1 b_2}{(a_0 a_3^2 + a_1^2 a_4 - a_1 a_2 a_3)} \qquad \left(\frac{\sigma_{\dot{q}}^2}{2f_s}\right) \tag{10}$$

where $a_0, \ldots, a_4$ are coefficients of the quartic characteristic polynomial; these and b_2 are defined as

$$\begin{aligned} a_0 &= 1 \qquad a_1 = \omega_{\mathrm{LP}} \qquad a_2 = \omega_{\mathrm{LP}}a_d + a_p \\ a_3 &= \omega_{\mathrm{LP}}a_p + a_I \qquad a_4 = \omega_{\mathrm{LP}}a_I \qquad b_2 = -\omega_{\mathrm{LP}}^2 a_d^2 \end{aligned} \tag{11}$$

For details of deviation of Eq. (10), see [2]. Standard deviation of the image angle due to quantization rate noise is thus given by σ_ε from Eq. (10). The variance results Eqs. (9) and (10) will be illustrated in Sec. V.

III. Attitude Determination with Misaligned Gyros and Star Trackers

Our objective in this section is to determine the steady-state bias and variance of the attitude estimation error $\tilde{\theta}_y$ when the attitude estimator employs measurements from the misaligned gyros and star trackers.

In practice, gyros, star trackers, and imaging sensors are somewhat misaligned from their ideal orientation due to installation imprecision, launch impacts, and time-varying thermal gradients in orbit. These misalignments can be estimated with an alignment Kalman filter [10], but in its absence, it is not clear how the attitude estimation error $\tilde{\theta}_y$ and the image angle ε are affected by the misaligned, uncalibrated gyros and star trackers. One suspects in this circumstance the inertial attitude estimate $\hat{\theta}_y$ would be relative to a misaligned inertial frame instead of the true inertial frame, and therefore the estimated pointing commands $\hat{\theta}_{yc}$ would be relative to this misaligned inertial frame also, provided there are no other

relative position estimation error sources. As a result, the focal plane image angle estimate, that is, the control error signal $\hat{\varepsilon} = \hat{\theta}_{yc} - \hat{\theta}_y$ in Fig. 1, would be, intuitively, independent of the gyros and star tracker misalignments. Our objective in this paper is to validate this intuition. The uncalibrated imaging sensor's own misalignment with the optical bench or spacecraft frame will, of course, cause a bias error in pointing that one will be able to estimate from the innovation using an adaptive relative navigation Kalman filter [9,11] but we will not pursue this topic here.

A. State-Space Model of Attitude Estimation with Misaligned Gyros

Following [10] and considering a single-axis again, the y_b axis of the spacecraft, the y gyro is assumed to be misaligned by a small angle δ_{yx} in the $x_b y_b$ plane and a small angle δ_{yz} in the $y_b z_b$ plane. Then the rate input to the y gyro is

$$\omega_{y,\text{input}} = \omega_y - \delta_{yx}\omega_x + \delta_{yz}\omega_z \tag{12}$$

where $\boldsymbol{\omega} = [\omega_x; \omega_y; \omega_z]$ is the spacecraft angular rate in the spacecraft frame. We will now develop a recursive model of the attitude measurement process of this gyro after Markley and Reynolds [3]. A gyro measures the spacecraft attitude at a very high sampling frequency (200 Hz in Fig. 1). The $(k+1)$th sample of the spacecraft y attitude is given in terms of the kth sample by

$$\theta_{y,k+1} = \theta_{y,k} + \Delta\theta_{y,k+1} \tag{13}$$

where $\Delta\theta_{y,k+1}$ is the true incremental change in the y attitude in one sample period, to be measured by the y gyro. Recalling Eq. (12), the $(k+1)$th angle actually measured by the misaligned gyro before quantization is

$$\phi_{y,k+1} = \phi_{y,k} + \tau b_k + \beta_k + \Delta\theta_{y,k+1} - \delta_{yx}\Delta\theta_{x,k+1} + \delta_{yz}\Delta\theta_{z,k+1} \tag{14}$$

where $\tau =$ the sample period of this recursive process, $b_k =$ the gyro drift rate, $\beta_k =$ the incremental random walk plus an angle due to the drift acceleration, and $\Delta\theta_{x,k+1}$ and $\Delta\theta_{z,k+1}$ are the incremental spacecraft attitude angles about the spacecraft x axis and z axis due to the orthogonal rates ω_x and ω_z. The gyro measures the last three terms in Eq. (14) as one quantity. Because of quantization, the gyro output angle will be

$$\phi_{y,k+1,\text{meas}} = \phi_{y,k+1} + \nu_{q,k} \tag{15}$$

where $\nu_{q,k}$ is the quantization error.

Because the mean and variance analysis of the attitude estimation error must be independent of the spacecraft attitude dynamics, the true incremental angle $\Delta\theta_{y,k+1}$ is determined in terms of the quantized gyro measurements $\phi_{y,k+1,\text{meas}}$ by substituting $\phi_{y,k+1}$ from Eq. (14) in the right side of Eq. (15), expressing $\Delta\theta_{y,k+1}$ in terms of other quantities, and then substituting $\Delta\theta_{y,k+1}$ in Eq. (13). We then obtain the following recursive equations that do not involve $\Delta\theta_y$:

$$\theta_{y,k+1} = \theta_{y,k} + \phi_{y,k+1,\text{meas}} - \phi_{y,k} - \tau b_k - \beta_k - \delta_{k+1} - \nu_{q,k} \tag{16a}$$

$$\phi_{y,k+1} = \phi_{y,k+1,\text{meas}} - \nu_{q,k} \tag{16b}$$

$$b_{k+1} = b_k + \alpha_k \tag{16c}$$

where a gyro measurement is now an input; the third equation above models the change in the drift rate with α_k as an increment, and the error angle δ_{k+1} abbreviates the last two terms in Eq. (14)

$$\delta_{k+1} = -\delta_{yx}\Delta\theta_{x,k+1} + \delta_{yz}\Delta\theta_{z,k+1} \tag{17}$$

For further analysis, Eqs. (16) are written in the state-space form as

$$\begin{bmatrix} \theta_{y,k+1} \\ b_{k+1} \\ \phi_{y,k+1} \end{bmatrix} = \begin{bmatrix} 1 & -\tau & -1 \\ 0 & 1 & 0 \\ 0 & 0 & 0 \end{bmatrix} \begin{bmatrix} \theta_{y,k} \\ b_k \\ \phi_{y,k} \end{bmatrix} + \begin{bmatrix} 1 \\ 0 \\ 1 \end{bmatrix} \phi_{y,k+1,\text{meas}} + \begin{bmatrix} -\beta_k - v_{q,k} \\ \alpha_k \\ -v_{q,k} \end{bmatrix} - \begin{bmatrix} \delta_{k+1} \\ 0 \\ 0 \end{bmatrix} \tag{18}$$

or, in compact notations, it is written as

$$\boldsymbol{x}_{k+1} = \Phi \boldsymbol{x}_k + [1 \quad 0 \quad 1]^T \phi_{y,k+1,\text{meas}} + \boldsymbol{w}_k - \boldsymbol{\Delta}_{k+1} \tag{19}$$

where the definition of each symbol in Eq. (19) is apparent by correspondence with Eq. (18).

The attitude estimation model for the y axis used in the attitude estimator is unaware of the gyro misalignments and the angle input δ_{k+1} from orthogonal axes. Also, the mean of the noise vector $\boldsymbol{w}_k$ in Eq. (29) is zero. Hence, the attitude estimation model is

$$\hat{\boldsymbol{x}}_{k+1} = \Phi \hat{\boldsymbol{x}}_k + [1 \quad 0 \quad 1]^T \phi_{y,k+1,\text{meas}} \tag{20}$$

where $\hat{\boldsymbol{x}}_k = [\hat{\theta}_{y,k};\ b_k;\ \hat{\phi}_{y,k}]$.

B. Attitude Estimation Error

Define the state estimation error vector [9] $\tilde{\boldsymbol{x}}_k = \hat{\boldsymbol{x}}_k - \boldsymbol{x}_k$, governed by an equation obtained by subtracting Eq. (19) from Eq. (20)

$$\tilde{\boldsymbol{x}}_{k+1} = \Phi \tilde{\boldsymbol{x}}_k - \boldsymbol{w}_k + \boldsymbol{\Delta}_{k+1} \tag{21}$$

Equation (21) is somewhat equivalent to the single-axis version of the three-axis Eq. (34) of [10]. Because of misalignment angles, $\tilde{\boldsymbol{x}}_k$ is not a zero-mean vector. Indeed, taking the mean of Eq. (21), we arrive at

$$\bar{\tilde{\boldsymbol{x}}}_{k+1} = \Phi \bar{\tilde{\boldsymbol{x}}}_k + \boldsymbol{\Delta}_{k+1} \tag{22}$$

where $\bar{\tilde{\boldsymbol{x}}}$ is the mean of $\tilde{\boldsymbol{x}}$.

To determine variance of the estimation error, define the zero-mean random error in $\tilde{\boldsymbol{x}}$ as [9] $\tilde{\tilde{\boldsymbol{x}}}_k = \tilde{\boldsymbol{x}}_k - \bar{\tilde{\boldsymbol{x}}}_k$. Then the equation governing $\tilde{\tilde{\boldsymbol{x}}}_k$ is obtained by subtracting Eq. (22) from Eq. (21)

$$\tilde{\tilde{\boldsymbol{x}}}_k = \boldsymbol{\Phi} \tilde{\tilde{\boldsymbol{x}}}_{k-1} - \boldsymbol{w}_{k-1} \tag{23}$$

The corresponding 3×3 covariance matrix propagation equation is $\boldsymbol{P}_k = \boldsymbol{\Phi} \boldsymbol{P}_{k-1} \boldsymbol{\Phi}^T + \boldsymbol{Q}$, as always, where the covariance matrix $\boldsymbol{P}_k = E(\tilde{\tilde{\boldsymbol{x}}}_k \tilde{\tilde{\boldsymbol{x}}}_k^T)$ and the process noise matrix $\boldsymbol{Q}$ is as defined in [3], involving $\sigma_u^2 =$ the power spectral density (rad^2/s^3) of the continuous-time acceleration of the drift, $\sigma_v^2 =$ the power spectral density (rad^2/s) of the continuous-time random walk rate, and $\sigma_q^2 (= q^2/12)$ is the discrete-time variance of the quantization error. Interestingly, the above mean and variance approach is different from the approach in [10] wherein one would use Eq. (21) directly for estimation and construct a cover covariance matrix of the spacecraft's rates and misalignment angles.

Because of a random walk, the variance of the spacecraft attitude estimate grows without bounds. To limit this variance, star tracker measurements are used, but a star tracker may also be misaligned. We consider this update process next.

C. Attitude Estimate and Variance Update with Misaligned Star Trackers

The spacecraft attitude measurement with star trackers may take place periodically, with a period T. Although not a requirement, here we assume that T is a multiple of the preceding sample period τ of the gyro attitude measurement process. In particular, following [3], we assume that when $k = n$, $T = n\tau$, a star tracker measures instantly the spacecraft attitude and furnishes

$$z_{\rm st} = \theta_{y,n} + \delta_{{\rm st},y} + \nu_{\rm st} \tag{24}$$

where $\theta_{y,n}$ is the true spacecraft attitude about the inertial y axis when $k = n$; $\delta_{{\rm st},y}$ is an unknown bias error in the star tracker measurement due to its misalignments, and $\nu_{\rm st}$ is a zero-mean white noise with variance $\sigma_{\rm st}^2$ contaminating the star tracker measurements. The gyro estimate of the spacecraft attitude $\hat{\theta}_{y,n}(-)$ at $t = n\tau$ just before the star tracker measurement is obtained from the state vector estimate $\hat{\boldsymbol{x}}_n(-)$, Eq. (20). The vector $\hat{\boldsymbol{x}}_n(-)$ is updated to $\hat{\boldsymbol{x}}_n(+)$ with the star tracker measurement $z_{\rm st}$, thus

$$\hat{\boldsymbol{x}}_n(+) = \hat{\boldsymbol{x}}_n(-) + \boldsymbol{K}_{\rm ss}[z_{\rm st} - \hat{\theta}_{y,n}(-)] \tag{25}$$

where $\boldsymbol{K}_{\rm ss}$ is the (3×1) Kalman gain vector of the steady-state attitude determination Kalman filter; see [1,3] for steady-state values of the Kalman gains.

To evaluate the mean and the variance of the state vector estimation error after the star tracker measurement update and to propagate them further with gyro measurements, we substitute the star tracker measurement $z_{\rm st}$, Eq. (24), in Eq. (25), define the preupdate spacecraft attitude estimation error $\tilde{\theta}_{y,n}(-) \triangleq \hat{\theta}_{y,n}(-) - \theta_{y,n}$ that emerges in the innovation, and subtract the true state vector $\boldsymbol{x}_n$ from both sides of the equation. We then arrive at the state estimation error update equation

$$\tilde{\boldsymbol{x}}_n(+) = \tilde{\boldsymbol{x}}_n(-) + \boldsymbol{K}_{\rm ss}[\delta_{{\rm st},y} + \nu_{\rm st} - \tilde{\theta}_{y,n}(-)] \tag{26}$$

The mean of this state vector estimation error update equation is

$$\bar{\tilde{\boldsymbol{x}}}_n(+) = \bar{\tilde{\boldsymbol{x}}}_n(-) + \boldsymbol{K}_{\rm ss}[\delta_{{\rm st},y} - \bar{\tilde{\theta}}_{y,n}(-)] \tag{27}$$

To update the variance of $\tilde{\boldsymbol{x}}_n$, the mean $\bar{\tilde{\boldsymbol{x}}}_n(+)$ is subtracted from $\tilde{\boldsymbol{x}}_n(+)$. Recalling the definition $\tilde{\tilde{\boldsymbol{x}}}_k = \tilde{\boldsymbol{x}}_k - \bar{\tilde{\boldsymbol{x}}}_k$, we arrive at the following update equation of the zero-mean estimation error vector $\tilde{\tilde{\boldsymbol{x}}}_n$:

$$\tilde{\tilde{\boldsymbol{x}}}_n(+) = \tilde{\tilde{\boldsymbol{x}}}_n(-) + \boldsymbol{K}_{\rm ss}[\nu_{\rm st} - \tilde{\tilde{\theta}}_{y,n}(-)] \tag{28}$$

where the zero-mean estimation error $\tilde{\tilde{\theta}}_{y,n}(-)$ is defined as $\tilde{\tilde{\theta}}_{y,n}(-) = \tilde{\theta}_{y,n} - \bar{\tilde{\theta}}_{y,n}$. Postmultiply Eq. (28) with its own transpose and perform its expectation operation. The following covariance update equation then follows:

$$\begin{aligned}\boldsymbol{P}_n(+) &= \boldsymbol{P}_n(-) - \boldsymbol{P}_{n,1}(-)\boldsymbol{K}_{\rm ss}^T - \boldsymbol{K}_{\rm ss}\boldsymbol{P}_{n,1}^T(-) \\ &\quad + \boldsymbol{K}_{\rm ss}\boldsymbol{K}_{\rm ss}^T[P_{n,11}(-) + R_{\rm st}]\end{aligned} \tag{29}$$

where

$$\boldsymbol{P}_{n,1}(-) = E\langle\tilde{\tilde{\boldsymbol{x}}}_n(-)\tilde{\tilde{\boldsymbol{\theta}}}y, n(-)\rangle = \text{the first column of } \boldsymbol{P}_n(-) \tag{30a}$$

$$\boldsymbol{P}_{n,11}(-) = E\langle\tilde{\tilde{\boldsymbol{\theta}}}_{y,n}^2(-)\rangle = (1,1) \text{ element of } \boldsymbol{P}_n(-) \tag{30b}$$

and $R_{\rm st}$ is the variance of the star tracker measurement noise $\nu_{\rm st}$. Note that the above update process maintains symmetry of the covariance matrix $\boldsymbol{P}_n$ because Eq. (29) is of a Joseph form. After the above update, the gyro measurement process continues recursively for the next $k = 0, 1, \ldots, n$ samples with the sample period τ, and the star tracker measurement and update recurs at $t = T$.

D. Steady-State Pre- and Postupdate Mean Attitude Estimation Error

One can derive literal steady-state mean of the attitude estimation error from the previous recursive attitude determination process. This steady-state process is portrayed in Fig. 2 where the index $k = n$ is reset to $k = 0$ at every star tracker measurement epoch. Our objective now is to determine the pre- and postupdate mean attitude estimation error in terms of the gyro and star tracker misalignments.

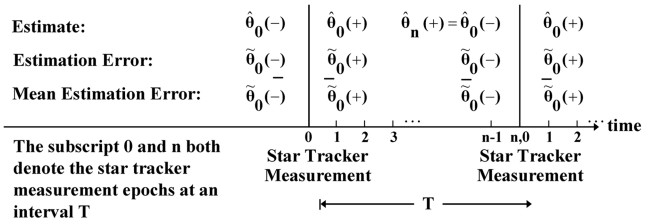

Fig. 2 Single-axis steady-state attitude determination Kalman filter: pre- and postupdate mean attitude estimation errors with a misaligned star tracker measurement.

In the state vector estimate $\hat{\boldsymbol{x}}_k$, the first element is the spacecraft attitude estimate $\hat{\theta}_{y,k}$. So the first row of Eq. (26) is

$$\tilde{\theta}_0(+) = \tilde{\theta}_0(-) + k_\theta[\delta_{\rm st} + \nu_{\rm st} - \tilde{\theta}_0(-)] \tag{31}$$

where the subscript n is replaced with "0," the subscript y is dropped from θ_y for clarity, and k_θ is the Kalman gain associated with θ_y. The steady-state Kalman gain k_θ is [3] $k_\theta = 1 - \zeta^{-2}$ where ζ depends on the standard deviations σ_u, σ_v, σ_q, and $\sigma_{\rm st}$ of the gyro and the star tracker noises, gyro sample period τ, and the star tracker measurement update interval T. Therefore, Eq. (31) can be rewritten as

$$\tilde{\theta}_0(+) = \zeta^{-2}\tilde{\theta}_0(-) + (1 - \zeta^{-2})(\delta_{\rm st} + \nu_{\rm st}) \tag{32}$$

the mean of which would be

$$\bar{\tilde{\theta}}_0(+) = \zeta^{-2}\bar{\tilde{\theta}}_0(-) + (1 - \zeta^{-2})\delta_{\rm st} \tag{33}$$

Over the interval T from $k = 0$ to $k = n$, due to misalignment angles of the y gyro and orthogonal rates of the spacecraft, the y gyro accumulates an angular error of

$$\Delta_n \triangleq -\delta_{yx}\int_0^T \omega_x \, {\rm d}t + \delta_{yz}\int_0^T \omega_z \, {\rm d}t = \sum_{k=0}^{n-1} \delta_{k+1} \tag{34}$$

From $t = 0$ to $t = n\tau$, the attitude estimation error grows from $\tilde{\theta}_0(+)$ to

$$\tilde{\theta}_n(+) = \tilde{\theta}_0(+) + \Delta_n + (b - \hat{b})T + \nu_{\rm rw}(T) + \nu_q \tag{35}$$

where $\hat{b}$ is the drift rate estimate, $\nu_{\rm rw}(T)$ is the random walk at $t = T$, and ν_q is the quantization noise. Note that unlike the random walk, the quantization noise does not accumulate or grow. Because the random quantities in Eq. (35) have zero mean, the mean of $\bar{\tilde{\theta}}_n(+)$ would be

$$\bar{\tilde{\theta}}_n(+) = \bar{\tilde{\theta}}_0(+) + \Delta_n \tag{36}$$

In steady state, $\bar{\tilde{\theta}}_n(+) = \bar{\tilde{\theta}}_0(-)$; therefore, Eqs. (33) and (36) can be solved for the unknown pre- and postupdate mean estimation errors, arriving at

$$\text{preupdate}: \ \bar{\tilde{\theta}}_0(-) = (1 - \zeta^{-2})^{-1}\Delta_n + \delta_{\rm st} \tag{37a}$$

$$\text{postupdate}: \ \bar{\tilde{\theta}}_0(+) = (\zeta^2 - 1)^{-1}\Delta_n + \delta_{\rm st} \tag{37b}$$

each expressed exclusively in terms of the gyro/star tracker misalignment angles. Clearly, if the misalignment angles δ_{yx}, δ_{yz}, and $\delta_{{\rm st},y}$ were all zero, the above two means would be zero also.

The nonzero mean errors developed above cause relative position and relative velocity estimation errors, which in turn cause pointing and rate command estimation errors, according to the signal path shown in Fig. 1.

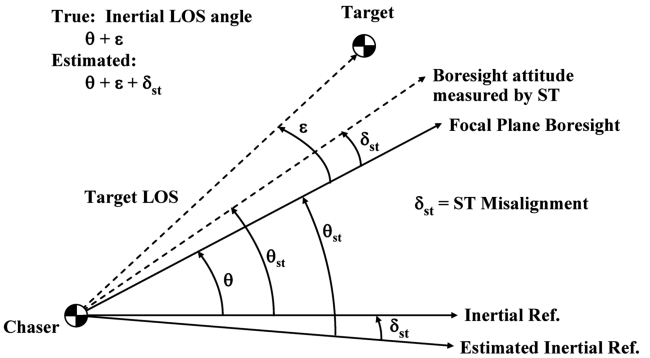

Fig. 3 True inertial angles of the focal plane boresight and target, and measurement with a misaligned star tracker (ST).

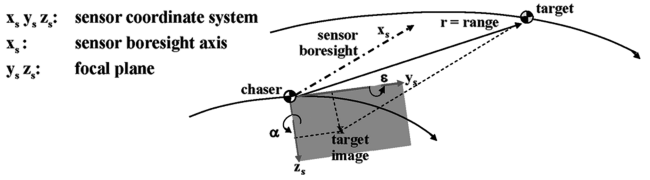

Fig. 4 Sensor measurements for relative navigation of the chaser: focal plane at the vehicle center of mass and aligned perfectly.

E. Attitude Estimation Error Affecting Relative Navigation

Figure 3 illustrates how the star tracker misalignment affects the focal plane measurement about the y axis. Suppose the focal plane boresight is oriented at an angle θ from an inertial reference, and the target is located at an elevation angle ε from the focal plane boresight. Then, the true inertial line-of-sight angle of the target is $(\theta + \varepsilon)$. The angle θ is measured by a star tracker which is misaligned about the y axis by δ_{st} such that the measurement is $\theta_{\text{st}} = \theta + \delta_{\text{st}}$ per Eq. (24) with zero random noise. Because the focal plane boresight attitude in the inertial frame is θ, the measurement θ_{st} is effectively from an estimated inertial reference at the misalignment angle δ_{st} from the true inertial reference, as shown in Fig. 3. The apparent inertial line-of-sight angle of the target is thus $\theta_{\text{st}} + \varepsilon = \theta + \delta_{\text{st}} + \varepsilon$.

A vector/matrix counterpart of the above scalar representation affecting relative navigation will be formulated now. Figure 4 depicts a sensor focal plane whose center is hypothetically at the mass center of the chaser satellite. In the sensor frame $x_s\ y_s\ z_s$, with the x_s axis as the sensor boresight, the focal plane azimuth and elevation line-of-sight (small) angles are $\alpha = \tan^{-1}(y_s/x_s)$, and $\varepsilon = \tan^{-1}(-z_s/x_s)$, and the client satellite is located at the relative position $\underline{\ell}_s = [x_s, y_s, z_s]^T$ in the sensor frame. In the inertial frame, the line-of-sight vector $\boldsymbol{\ell}$ from the chaser satellite to the client satellite is related to $\boldsymbol{\ell}_s$ via the inertial attitude direction cosine matrix $\boldsymbol{C}_{Is}$ of the sensor frame: $\boldsymbol{\ell}^{\mathsf{F}^I} = \boldsymbol{C}_{Is}\boldsymbol{\ell}_s$ where F^I denotes the inertial frame. For a relative navigation Kalman filter, the state vector of which is in inertial Cartesian coordinates [2], we require slopes of the angles α and ε with respect to the estimated LOS vector $\hat{\boldsymbol{\ell}}$. These slopes are related to the slopes in the sensor frame, thus [12]

$$\frac{\partial \alpha}{\partial \underline{\hat{\ell}}} = \hat{\boldsymbol{C}}_{Is}\frac{\partial \alpha}{\partial \hat{\boldsymbol{\ell}}_s}; \tag{38a}$$

$$\frac{\partial \varepsilon}{\partial \underline{\hat{\ell}}} = \hat{\boldsymbol{C}}_{Is}\frac{\partial \varepsilon}{\partial \hat{\boldsymbol{\ell}}_s} \tag{38b}$$

where $\hat{\boldsymbol{C}}_{Is}$ is the estimated inertial attitude of the sensor, and $\hat{\boldsymbol{\ell}}$ is the estimate of the relative position $\boldsymbol{\ell}_s$ of the target in the sensor frame. The attitude determination Kalman filter provides $\hat{\boldsymbol{C}}_{Is}$. Because the gyro/star tracker misalignment angles affect the estimate $\hat{\boldsymbol{C}}_{Is}$, clearly the relative position and relative velocity estimates, $\hat{\boldsymbol{\ell}}$ and $\dot{\hat{\boldsymbol{\ell}}}$, of the client from the chaser will be reckoned from the misaligned inertial frame, as in Fig. 3. As a side comment, we note that in our earlier work, [1], the slopes of the angles α and ε in the sensor frame in Eqs. (38) were transformed to the local-vertical–local-horizontal (LVLH) orbit frame. But this frame is not adopted here because the Clohessey–Wiltshire relative equations of motion in this frame cause significant relative navigation errors at the 10–20-km range [13] where an imaging sensor begins to sense a target satellite.

IV. Pointing and Tracking Commands

When the relative position vector $\boldsymbol{\ell}$ of the target satellite from the chaser satellite has been estimated with a relative navigation Kalman filter [2] or otherwise, it is used to calculate the pointing command to bring the target to the focal plane center. Suppose the focal plane boresight unit vector $\boldsymbol{b}$ is initially aligned with the inertial x axis of the frame in which $\boldsymbol{\ell}$ is estimated; then [14] shows that the quaternion command to align the boresight $\boldsymbol{b}$ with $\boldsymbol{\ell}$ is

$$q_{cI} = \frac{1}{\sqrt{2(1 + \boldsymbol{b}\cdot\boldsymbol{u})}} \qquad [\boldsymbol{b}\times\boldsymbol{u};\ 1 + \boldsymbol{b}\cdot\boldsymbol{u}] \tag{39}$$

where $\boldsymbol{u}$ is the unit vector along $\boldsymbol{\ell}(\boldsymbol{u} = \boldsymbol{\ell}/|\boldsymbol{\ell}|)$. Clearly, if there is some estimation error in the estimate $\hat{\boldsymbol{\ell}}$ wherefrom the unit vector $\hat{\boldsymbol{u}}$ is calculated, the estimated pointing command $\hat{q}_{cI}$ will have some estimation error.

While the pointing command (39) is used to acquire and then track the target, the rate command may be used to track the target with greater precision. Knowing the relative velocity vector $\dot{\boldsymbol{\ell}}$, the angular rate command to track the target is [1]

$$\underline{\omega}_{cI} = (\boldsymbol{\ell}\times\dot{\boldsymbol{\ell}})/(\boldsymbol{\ell}\cdot\boldsymbol{\ell}) \tag{40}$$

where the estimates of $\boldsymbol{\ell}$ and $\dot{\boldsymbol{\ell}}$ are known in the inertial frame. From the attitude control standpoint, the rate command $\boldsymbol{\omega}_{cI}$ needs to be known in the current body frame, however, so that the rate error $\boldsymbol{\omega}_e = \boldsymbol{\omega}_{cI} - \boldsymbol{\omega}_{bI}$ can be calculated for control in this frame (where $\boldsymbol{\omega}_{bI} =$ the spacecraft's inertial rate in the body frame). Therefore $\boldsymbol{\ell}$ and $\dot{\boldsymbol{\ell}}$ need to be transformed from the inertial frame to the current body frame and then substituted in Eq. (40).

V. Numerical Results and Discussion

A. Rendezvous Scenario Using Glide-Slope Guidance

To illustrate relative navigation and guidance for the rendezvous of one satellite with another using the imaging sensor pointing controller, Fig. 1, and to illustrate the controller's insensitivity to the gyro and star tracker misalignments, we developed a 9-degree of freedom (DOF) simulation: three translation DOF of the client satellite, and six translation and rotational DOF of the chaser satellite in a spherical plus J_2 gravity field. We consider a scenario shown in Fig. 5 where the chaser satellite is $\sim$19 km behind and 10 km below the target satellite at $t = 0$. The initial position and velocity of the two satellites were specified in the inertial frame using orbital elements. Because guidance improves the estimation process due to additional dynamics and accelerometer measurements, a 1/60 Hz (i.e., sampling period 60 s) glide-slope guidance [15] is employed. This guidance technique decreases relative velocity and position exponentially. The global positioning system (GPS)-based inertial navigation errors of the chaser satellite are simulated as exponentially correlated Markov processes with the following parameters[†] representing a precise positioning service of GPS [9,16]:

s.d. of bias in each axis = 5.1 m, time constant = 1/8 orbital period;

s.d. of horizontal random error = 1.4 m, time constant = 1 min;

s.d. of velocity random error = 0.07 m/s.

In 1800 s, the guidance system steers the chaser satellite to its final position [−1; 0; 1] km relative to the target in the target's

[†]Courtesy of D. Childers, The Boeing Company, Huntington Beach, California.

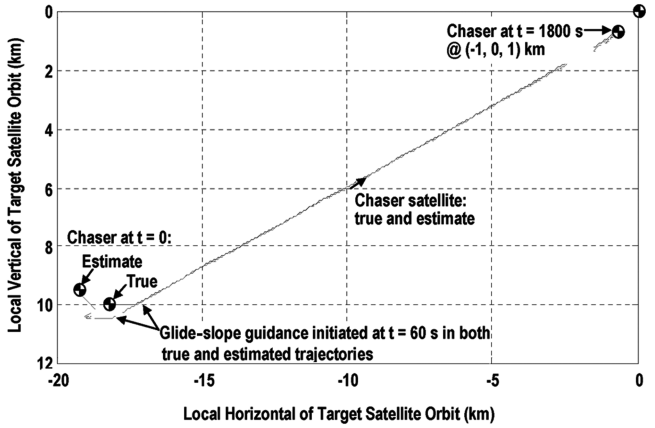

Fig. 5 A six-state relative inertial navigation: inertial propagation for relative navigation of target satellite.

instantaneous LVLH frame. Because the LVLH frames are convenient to visualize the motion of the chaser satellite relative to the target satellite, both true and estimated instantaneous LVLH frames of the two satellites are computed and used; the control system is based on inertial angles and inertial rates, however. The relative position and velocity estimates of the chaser satellite have initial estimation errors equal to [1; 0.49; 0.49] km (Fig. 5) and [0.5; 0.5; 0.5] m/s. A 10-Hz relative navigation Kalman filter removes the large initial estimation error with the first few 1-Hz angle measurements by the imaging sensor. The details of this filter are presented in [1,2]. To isolate the effects of the gyro and star tracker misalignments, gyro drift, random walk, quantization and star tracker measurement noise are all ignored, although their variances are considered to determine the steady-state Kalman gains of the attitude estimator for blending the misaligned gyro and star tracker measurements. Only the imaging sensor random noise is included in the simulation. The glide-slope guidance commences at $t = 60$ s, and steers the spacecraft to its final position in 29 pulses, one pulse every 60 s, in the remaining 1740 s. This gliding motion on a slope (hence the name *glide slope*) in the target satellite orbit plane is depicted in Fig. 5.

B. Pointing and Rate Commands

Although for attitude control the inertial quaternion commands (39) and the inertial rate command vector (40) are used in the simulation, Euler angle commands and scalar rate commands are stated here for clarity and illustration. Assuming that the focal plane boresight is initially aligned with the x_I-inertial axis, and that the line-of-sight vector $\boldsymbol{\ell}$ in the inertial frame is $\boldsymbol{\ell}^{F_I} = [\ell_{xI};\ \ell_{yI};\ \ell_{zI}]$, the pointing commands about the inertial y_I axis and about the once-displaced z_I axis are [15] $\theta_{yI,c} = \arctan(-\ell_{zI}, \ell_{xI})$, and $\theta_{zI,c} = \arcsin(\ell_{yI}/\|\boldsymbol{\ell}\|)$, where $\|\boldsymbol{\ell}\| = (\ell_{xI}^2 + \ell_{yI}^2 + \ell_{zI}^2)^{1/2}$. For rate command, the line-of-sight vector $\boldsymbol{\ell}$ would be $\boldsymbol{\ell}^{F_c} = [\ell_{xc};\ 0;\ 0]$ in the commanded body frame because the commanded focal plane boresight axis x_c is pointed at the target. Expressing the line-of-sight inertial velocity vector $\dot{\boldsymbol{\ell}}$ in the commanded body frame as $\dot{\boldsymbol{\ell}}^{F_c} = [\dot{\ell}_{xc};\ \dot{\ell}_{yc};\ \dot{\ell}_{zc}]$, Eq. (40) yields these three components of the rate command in the commanded body frame: $\omega_{xc} = 0$, $\omega_{yc} = -\dot{\ell}_{zc}/\ell_{xc}$, and $\omega_{zc} = \dot{\ell}_{yc}/\ell_{xc}$. The true and the estimated pointing commands $(\theta_{yI,c}, \theta_{zI,c})$ and the rate commands $(\omega_{yc}, \omega_{zc})$ in the presence of imaging sensor noise and GPS-based inertial navigation errors are illustrated in Figs. 6a and 6b, respectively, for

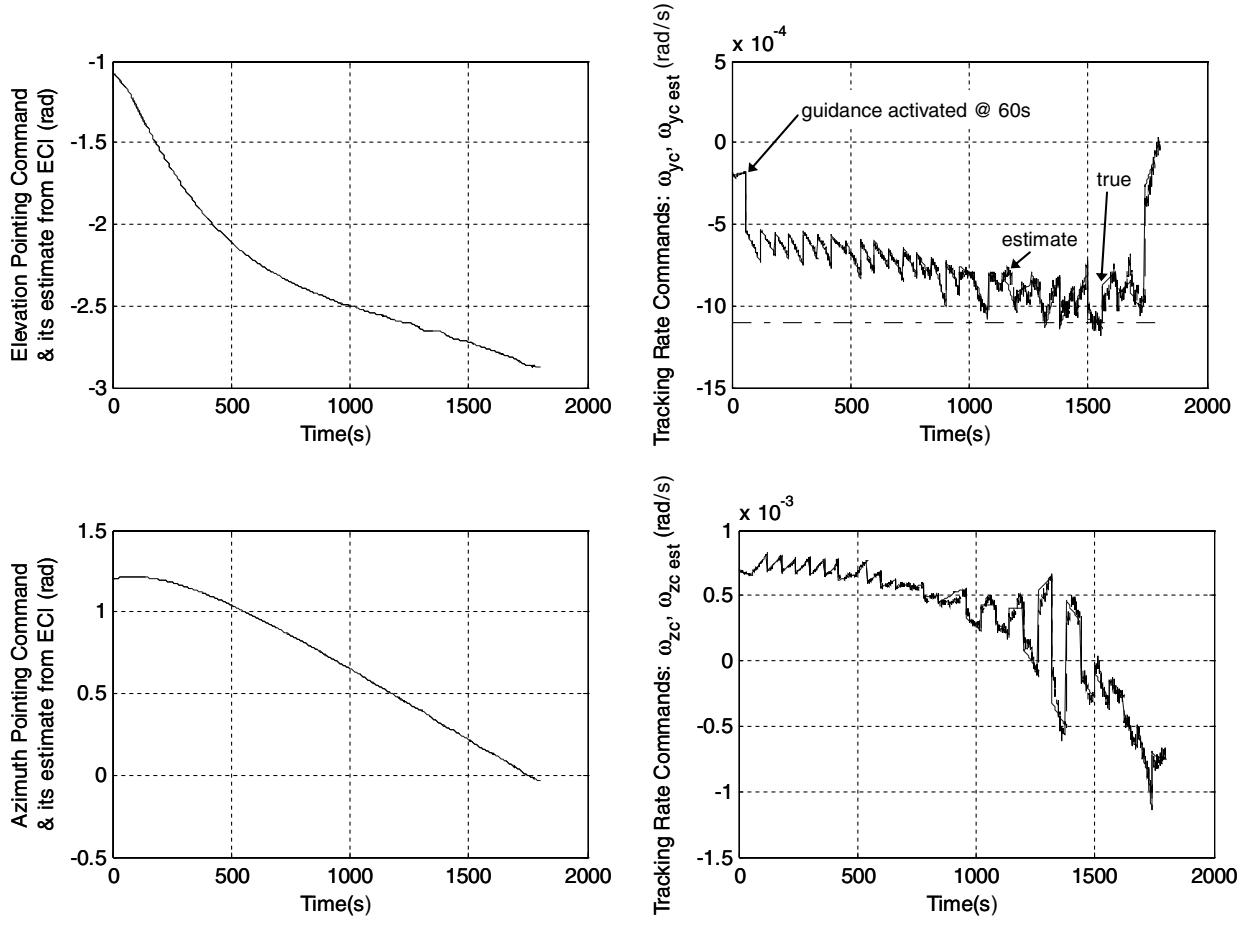

a) b)

Fig. 6 a) True and estimated inertial pointing commands: elevation (I rotation about the *y* axis), and azimuth (II rotation about the *z* axis); b) true and estimated inertial rate commands about the sensor focal plane *y* and *z* axes.

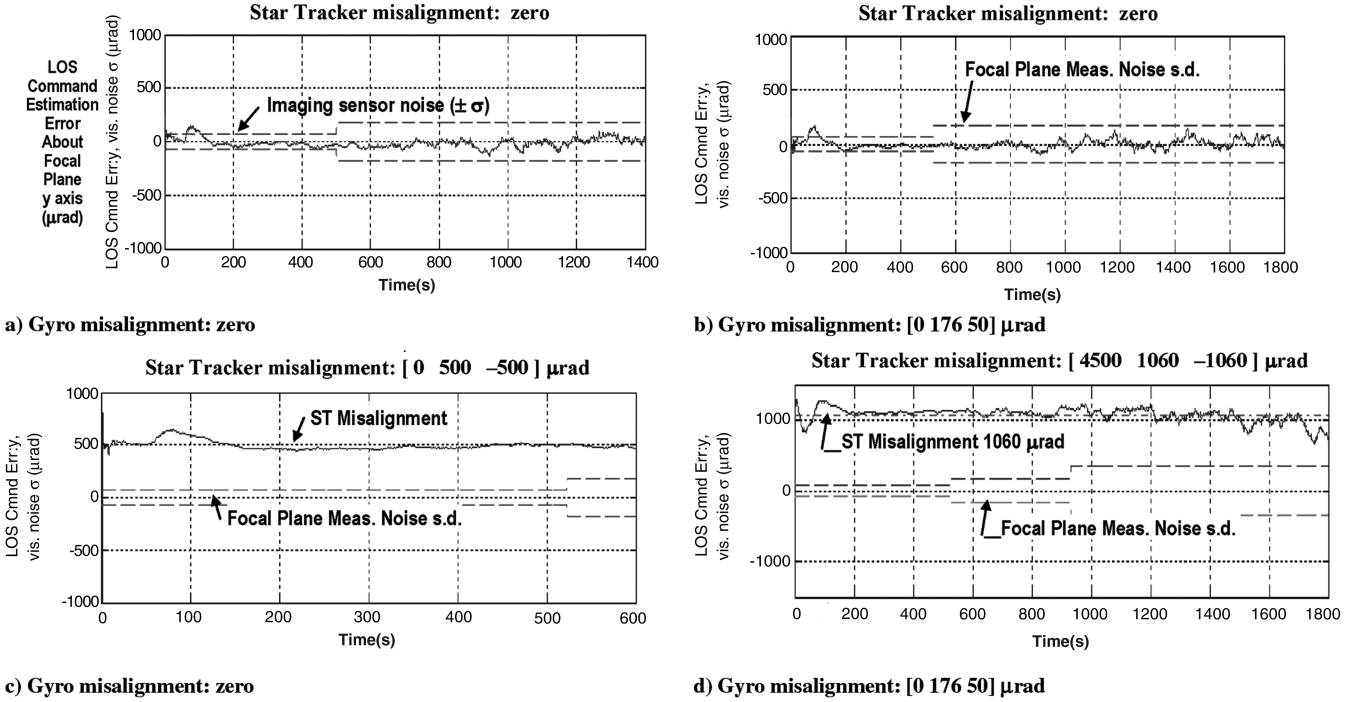

Fig. 7 LOS command estimation errors about focal plane *y* axis.

the rendezvous scenario in Fig. 5. The change in the slopes of the pointing commands and the discrete jumps in the rate commands every 60 s starting from $t = 60$ s in Figs. 6a and 6b are due to the incremental velocity changes caused by the guidance thrusters. Note that the rate commands are of the same order of magnitude for all 1800 s because the guidance decreases periodically and exponentially both the relative velocity and the relative range with a pulse every 60 s. This limits the rate command estimation errors. The high-frequency noise apparent in the estimated rate commands is due to the sensor noise and the inertial navigation error mentioned previously, attenuated some by the relative navigation Kalman filter.

C. Line-of-Sight Command Angle Estimation Errors due to Misalignments

In all subsequent figures, unless specifically noted, GPS-based inertial navigation errors are zeroed. The difference between the true and the estimated LOS commands in Fig. 6a is shown in Fig. 7 about the focal plane y axis for four different cases of the rendezvous scenario in Fig. 5: a) the gyros and the star tracker aligned with the focal plane frame perfectly; b) the gyros misaligned by [0; 176; 50] μrad but the star tracker aligned perfectly; c) the gyros aligned perfectly but the star tracker misaligned by [0; 500; -500] μrad; and d) the gyros misaligned by [0; 176; 50] μrad and the star tracker misaligned by [4500; 1060; -1060] μrad. In each case, the gyros are initialized with the star tracker measurements, and the star tracker measurements take place every 6 s. The command estimation errors are referenced from the true commanded focal plane orientation to the estimated commanded focal plane orientation; in the transformation matrix notation, we have $\boldsymbol{C}_{\hat{c}c} = \boldsymbol{C}_{\hat{c}I}\boldsymbol{C}_{Ic}$ where $C_{Ic} =$ the command-to-inertial transformation matrix, $\boldsymbol{C}_{\hat{c}I} =$ the inertial-to-estimated commanded focal plane transformation matrix, and $\boldsymbol{C}_{\hat{c}c} =$ the transformation matrix from the true to the estimated commanded orientation. The y- and z-command angle estimation errors are then $\tilde{\theta}_{yc} = \boldsymbol{C}_{\hat{c}}$ (3, 1) element and $\tilde{\theta}_{zc} = \boldsymbol{C}_{\hat{c}c}$ (1, 2) element. For the four cases defined above, Fig. 7 illustrates $\tilde{\theta}_{yc}$ and standard deviation σ_{img} of the imaging sensor measurement noise, which increases discretely as the range reduces with time. In case a of perfect alignment of the gyros and the star tracker with the focal plane, the error $\tilde{\theta}_{yc}$ is almost entirely well within $\pm\sigma_{\text{img}}$ as it should be because of the noise attenuation property of the relative navigation Kalman filter. In case b in which the gyros are misaligned by [0; 176; 50] μrad but the star tracker is aligned perfectly with the focal plane frame (recall that the star tracker measurements are used every 6 s in all cases), the attitude determination errors due to the gyro misalignments do not grow much with the spacecraft rates shown earlier in Fig. 6b, and the error $\tilde{\theta}_{yc}$ remains about the same as in case a. In case c, where the star tracker is misaligned by [0; 500; -500] μrad but the gyros are aligned perfectly (initialized with the star tracker measurements, however), the LOS command estimation error $\tilde{\theta}_{yc}$ is found to be biased by the star tracker misalignment angle 500 μrad, as intuition would suggest. Last, in case d, the gyros and

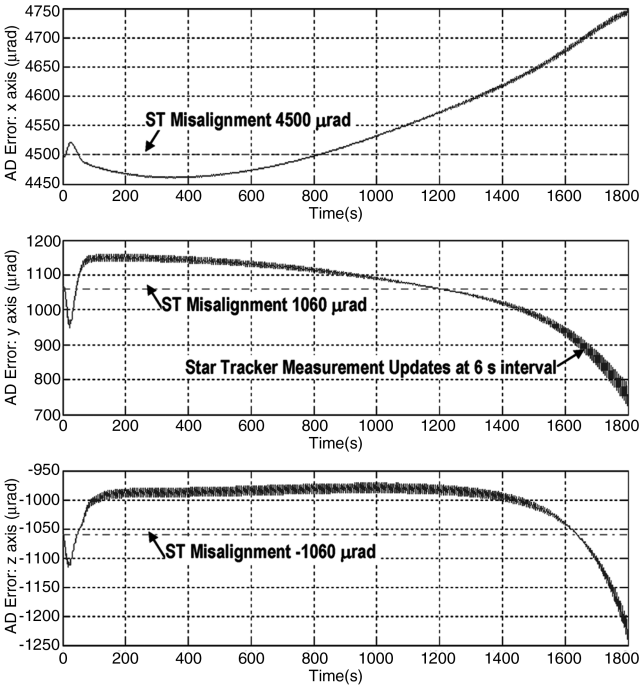

Fig. 8 Attitude estimation error of the Kalman filter in spacecraft frame due to gyro and star tracker misalignments: star tracker measurement interval: 6 s.

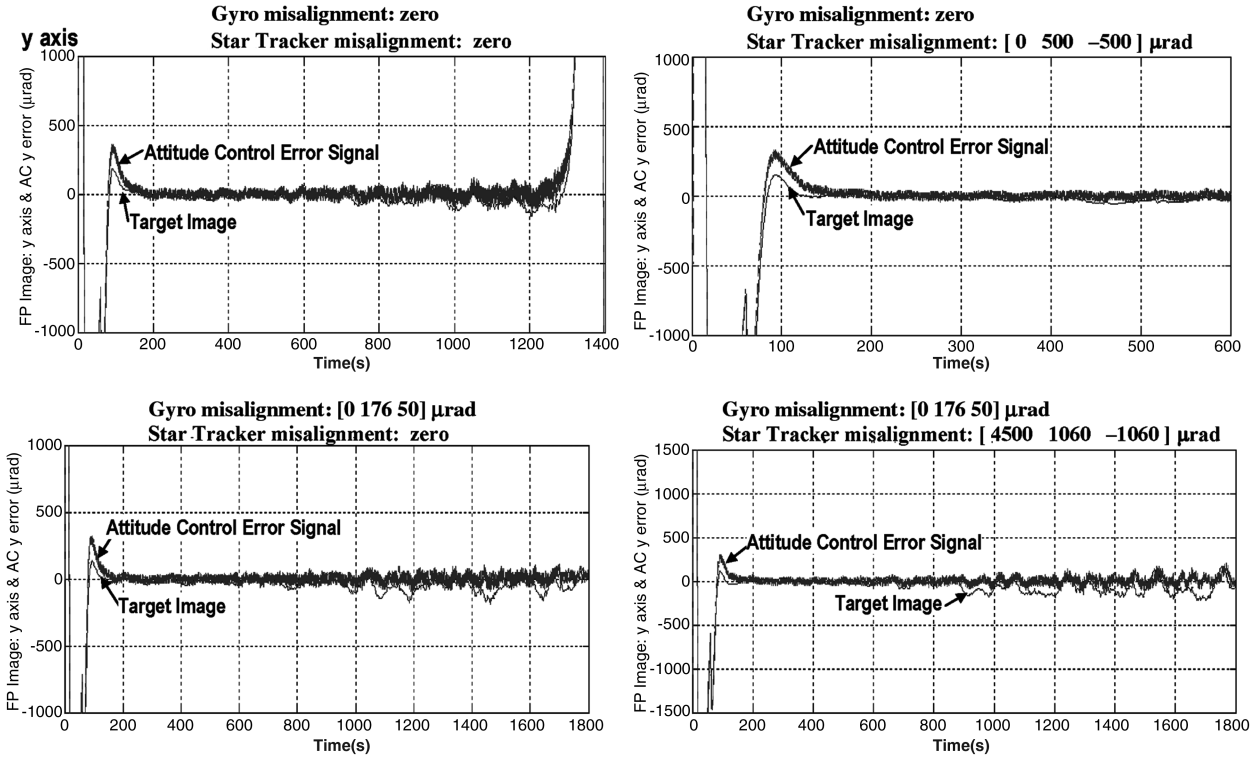

Fig. 9 *y* angle of the focal plane image and attitude control error signal about the *y* axis.

the star tracker are both misaligned, but $\tilde{\theta}_{yc}$ is essentially biased by the star tracker misalignment angle 1060 μrad. Not surprisingly, these results are similar to the attitude estimation error results of an uncalibrated Kalman filter in [10].

Figure 8, on the other hand, portrays attitude determination errors $[\tilde{\theta}_x;\ \tilde{\theta}_y;\ \tilde{\theta}_z]$ arising from the gyros and the star tracker misalignments of case d in Fig. 7d, with star tracker measurement updates every 6 s and a steady-state attitude determination Kalman filter unaware of the misalignments. In brief, the three-axis attitude determination errors accumulated during the star tracker measurement interval T, solely due to the gyro misalignments and the spacecraft rate $\boldsymbol{\omega} = [\omega_x;\ \omega_y;\ \omega_z]$, would be

$$\Delta_x = \delta_{xy}\int_0^T \omega_y\,\mathrm{d}t - \delta_{xz}\int_0^T \omega_z\,\mathrm{d}t \tag{41a}$$

$$\Delta_y = -\delta_{yx}\int_0^T \omega_x\,\mathrm{d}t + \delta_{yz}\int_0^T \omega_z\,\mathrm{d}t \tag{41b}$$

$$\Delta_z = \delta_{zx}\int_0^T \omega_x\,\mathrm{d}t - \delta_{zy}\int_0^T \omega_y\,\mathrm{d}t \tag{41c}$$

where each gyro's misalignment is modeled with two angles [10]. The angle Δ_n defined earlier by Eq. (34) is the same as Δ_y above. The high-frequency noise, more visible in $\tilde{\theta}_y$ and $\tilde{\theta}_z$ in Fig. 8, is due to the star tracker measurement updates every 6 s. The spacecraft's true rate $\boldsymbol{\omega}$ is not shown here for brevity, but the attitude determination error in Fig. 8 about each axis hovers near the star tracker misalignment angle for that axis. Therefore, we infer from Figs. 7 and 8 that when the estimated quaternion and the estimated commanded quaternion are multiplied to obtain the quaternion error, the three-axis counterpart of the single-axis control error signal $\hat{\varepsilon}$ in Fig. 1, the quaternion error would be free from the time-varying bias errors due to the gyro and the star tracker misalignment angles (shown in Fig. 10 for the *y* axis). Small zero-mean high-frequency errors seen in Figs. 7 and 8 would remain, attenuated some by the low bandwidth tracking controller.

D. Focal Plane Image Angle Insensitive to Misalignments

The attitude control error signal, $\hat{\varepsilon}$ in Fig. 1, is shown in Fig. 9 for the *y* axis for the same four cases. In addition, Fig. 9 shows the true focal plane image angle ε. It is remarkable that $\hat{\varepsilon}$ and ε are about the same for all four cases; $\hat{\varepsilon}$ is noisy as explained above but the gyros and the star tracker misalignment angles in cases b–d and the resulting bias errors seen in Fig. 8 have no influence on these variables. The image stays close to the focal plane center in all cases, as desired, despite the gyro/star tracker misalignments.

As the range between the two spacecraft diminishes, the pointing accuracy requirement for the focal plane of the imaging sensor relaxes, although the imaging sensor noise escalates because the target image illuminates a progressively larger pixel area. Figure 10 portrays the laser range finder (LRF) pointing requirement,[‡] the standard deviation of the sensor noise,[§] and the focal plane pointing accuracy versus the range between the two spacecraft for the above four cases. Curiously, as in Fig. 9, the pointing accuracy achieved by the controller is the same for all four cases, and the gyro/star tracker misalignments have no influence on it. The pointing requirement commencing from the range 12.5 km is met for all four cases.

E. Image Angle with GPS Inertial Navigation Errors

In the results so far (except those in Fig. 6), the inertial position and velocity of the chaser satellite is assumed to be known without errors. When these errors, specified earlier, are included, the pointing accuracy requirement using the same six-state relative inertial navigation filter is met only occasionally, as shown in Fig. 11. But these results are based on angle measurements only, ignoring the occasional range measurement that is made possible when the pointing accuracy requirement is momentarily met. The current relative navigation filter needs to be augmented to use these sporadic range measurements in conjunction with the azimuth and elevation angle measurements. Furthermore, to incorporate inertial navigation errors in the relative navigation formulation, a more complete Kalman filter model that encompasses orbit determination of both satellites with GPS receiver measurements might also be required.

[‡]Courtesy of J. LeCroy, The Boeing Company, Huntsville, Alabama.
[§]Courtesy of P. Scott, The Boeing Company, Anaheim, California.

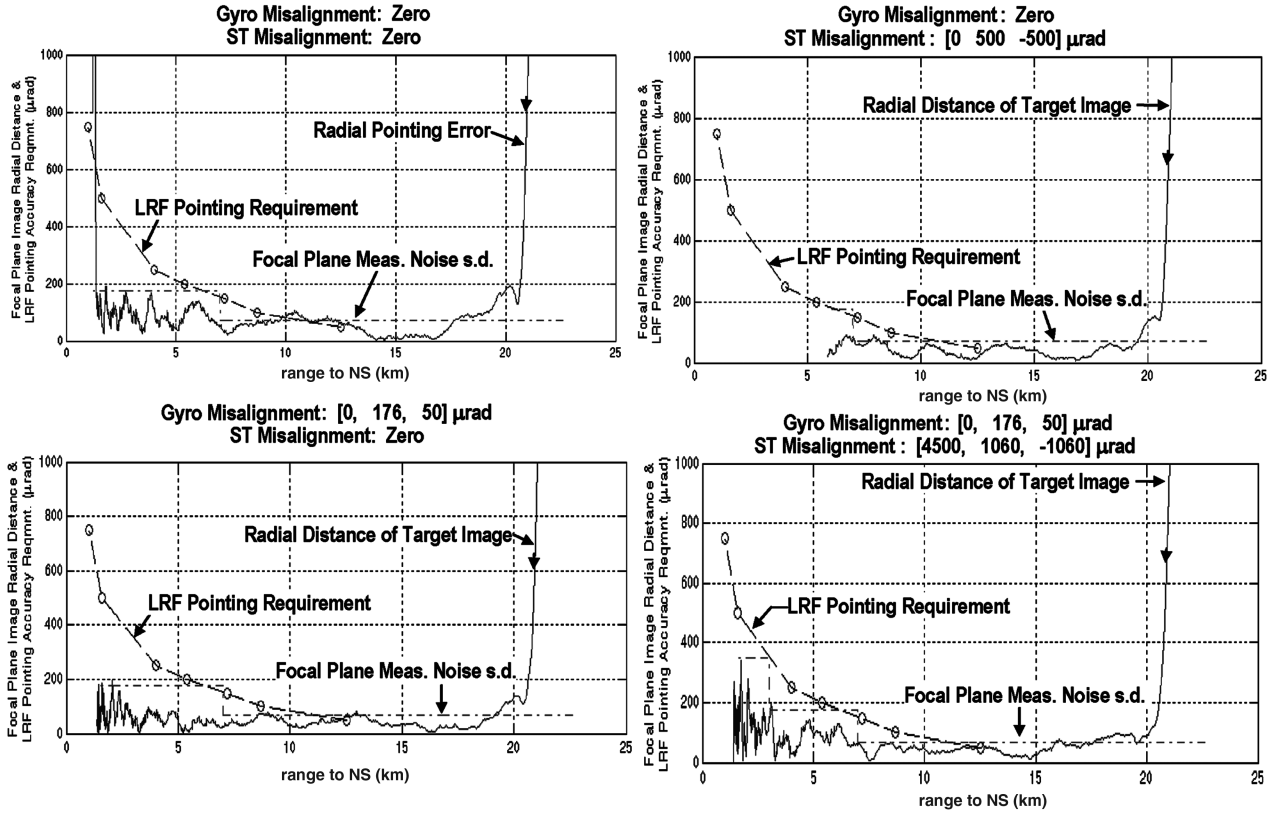

Fig. 10 Target image on the focal plane for zero misalignment and three gyro/star tracker misalignment cases.

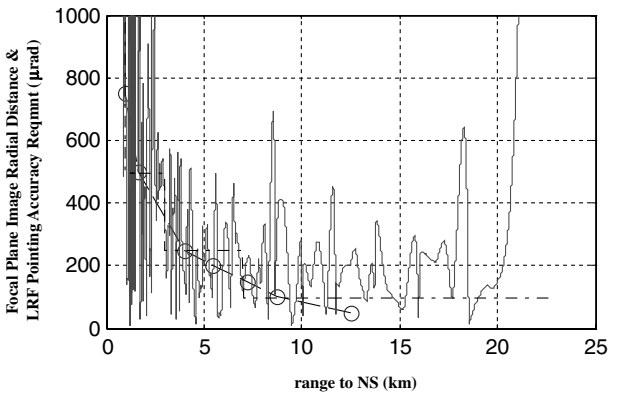

Fig. 11 Target image motion on the focal plane in the presence of SIGI navigation errors.

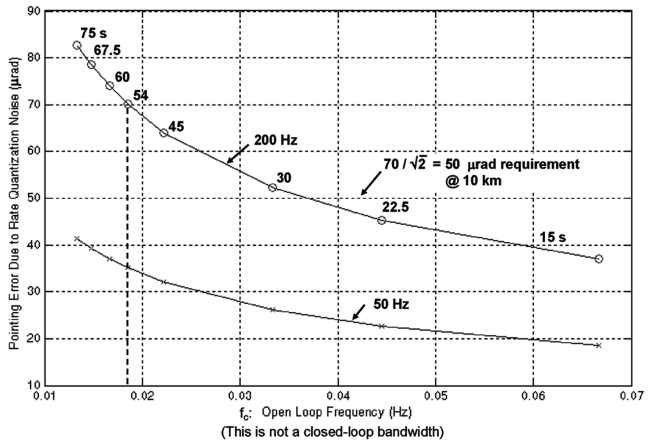

Fig. 12 Pointing error caused by quantization rate noise decreases as the PID controller bandwidth increases.

F. Steady-State Pointing Error due to Gyros and Star Tracker Random Noises

In the preceding time-domain simulation, we have ignored the zero-mean random noises of the gyros and star trackers. We will now illustrate the standard deviation of the steady-state zero-mean pointing error caused by these noise sources–the statistical analysis of Sec. II.

Suppose gyros measure spacecraft attitude with a quantization pulse $q = 5$ μrad. The corresponding standard deviation of the white noise would be $\sigma_q = 5/\sqrt{12} \approx 1.5$ μrad, and the quantization rate noise at 200 Hz gyro output would be $\sigma_{\dot{q}} = \sqrt{2}\,\sigma_q/0.005$ s$=$ 408 μrad/s. This noise is attenuated by a $\sim$10 Hz low-pass filter to $0.22\sigma_{\dot{q}} \approx 90$ μrad/s. (The factor 0.22 is determined by analyzing the response of the first-order low-pass filter $H_{\rm LP}$ in the discrete z domain.) If the gyro output is at 50 Hz, the filtered quantization rate noise would drop to $\sim$22 μrad/s. For various bandwidths of the proportional–integral–derivative controller for spacecraft pointing, specified in terms of the time period (15, 22.5, …, 75 s) of the associated second-order complex conjugate pole, Fig. 12 shows the image angle standard deviation σ_ε attributed to the filtered $\sigma_{\dot{q}}$, Eq. (10), versus the open-loop frequency $1/$(time period) for both 200 and 50-Hz gyro output. We observe that, for the open-loop frequency range considered in Fig. 12, σ_ε diminishes as the open-loop frequency (related to the closed-loop bandwidth) increases—a trend illustrated in [5]. We observe, too, that if the gyro output frequency is reduced to 50 Hz, the pointing error is halved. The gyro output frequency 50 Hz is acceptable because the closed-loop bandwidth of the PID controller is 0.06 Hz (corresponding to the 54 s period in Fig. 14) and it operates at a 25-Hz sampling frequency.

Next, the standard deviation of the steady-state pointing error owing to the zero-mean attitude determination error $\tilde{\theta}_y$, Eq. (9), is portrayed in Fig. 13 for the gyro parameters $\sigma_q = 1.5$ μrad, $\sigma_v = 0.75$ μrad/s$^{0.5}$, $\sigma_u = 4.0\text{e}-6$ μrad/s$^{3/2}$, the star tracker noise $\sigma_{\rm st} = 35$ μrad, and the star tracker measurement intervals $T = 1$, 15, and 300 s. For these parameters, the standard deviations $\sigma_{\tilde{\theta}}(-)$ of the attitude estimation error just before the star tracker measurement update at $T = 1$, 15, and 300 s are 5.4, 10.4, and 23.5 μrad,

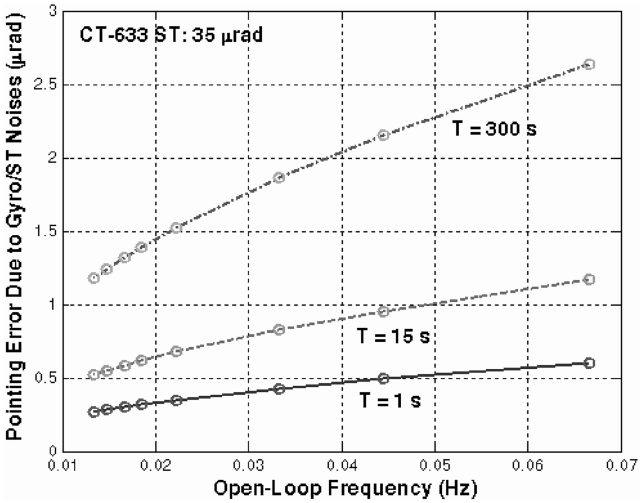

Fig. 13 Standard deviation of single-axis pointing error due to gyros and star tracker random errors.

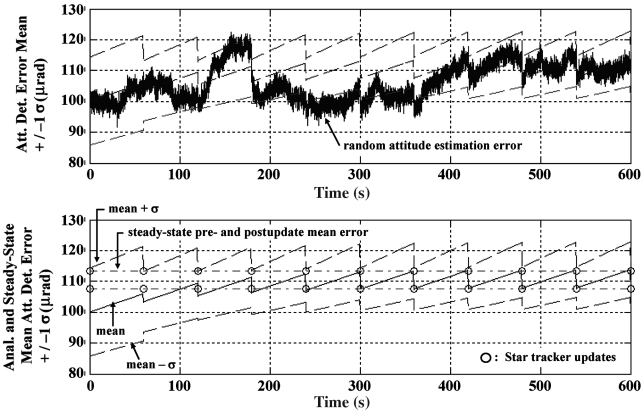

Fig. 14 Attitude estimation error, its mean and $\pm 1\sigma$ standard deviation, and steady-state pre- and postupdate mean errors: star tracker measurement interval 60 s.

respectively [1]. Standard deviation σ_ε of the closed-loop target image angle on the focal plane, shown in Fig. 13, is an order of magnitude smaller than $\sigma_{\tilde{\theta}}$ for the same T. We further observe that unlike the s.d. of the image angle jitter due to the quantization rate noise, σ_ε in Fig. 13 increases with the open-loop frequency and with T. But these errors in Fig. 13 are much smaller than the errors due to the quantization rate noise in Fig. 12.

G. Attitude Estimation Errors with Misalignments and Zero-Mean Noises of Gyros and Star Trackers

Earlier, Fig. 8 illustrated attitude estimation errors due to the misaligned gyros and star trackers, with the focal plane tracking a client satellite but without zero-mean random errors of the gyros and the star trackers. We now illustrate the analysis in Sec. III. Consider a single-axis (y-axis) gyro and a star tracker with the random noise parameters stated in the previous paragraph. In addition, the y gyro is misaligned by angles 50, 50 μrad about the x and z axes, and the star tracker is misaligned by 100 μrad. The gyro-measured attitude is initialized with a star tracker measurement, and the spacecraft rotates with constant rates [0.001, 0.001] rad/s about the x and z axes. The upper part of Fig. 14 then illustrates the y-attitude estimation error in the presence of all random and misalignment errors. In addition, the figure illustrates the mean attitude estimation error $\bar{\tilde{\theta}}_y$ and $\bar{\tilde{\theta}}_y \pm \sigma_{\bar{\tilde{\theta}}}$, where $\sigma_{\bar{\tilde{\theta}}} = [E(\bar{\tilde{\theta}}_y^2)]^{1/2}$, and $\bar{\tilde{\theta}}_y = \bar{\theta}_y - \bar{\tilde{\theta}}_y$, as predicted by the recursive analysis in Sec. III. We observe that the random attitude estimation error is bounded well by $\bar{\tilde{\theta}}_y \pm \sigma_{\bar{\tilde{\theta}}}$. The star tracker measurement updates take place at an interval of 60 s, and the statistical estimation errors have the steady sawtooth shapes. The lower part of Fig. 14 corroborates the steady-state analysis, illustrating that the mean attitude estimation error $\bar{\tilde{\theta}}_y(+)$, after some initial transients, varies as a sawtooth function between the steady-state preupdate $\bar{\tilde{\theta}}_0(-)$ and the steady-state postupdate $\bar{\tilde{\theta}}_0(+)$ mean estimation errors.

VI. Conclusions

A pointing and tracking controller for an imaging sensor on a chaser satellite to rendezvous with a target satellite is presented. Its remarkable attribute is that its pointing accuracy is independent of the misalignment of the gyros and star tracker inertial sensors with the optical axis of the imaging sensor. This transpires because the misalignments merely introduce a slightly disoriented inertial frame wherefrom both the attitude command estimate and the focal plane attitude estimate are measured. So, in the end, the difference of these two attitude estimates, the attitude error signal, inputted to the attitude controller is still estimated from an estimated imaging sensor boresight, not from the disoriented inertial frame. Consequently, the pointing accuracy of the imaging sensor is just the same whether gyros and star trackers are misaligned with the imaging sensor axes or not—a remarkable and very useful conclusion, but perhaps evident to some intuitively ab initio.

References

[1] Hablani, H. B., "Autonomous Relative Navigation, Attitude Determination, Pointing and Tracking for Spacecraft Rendezvous," AIAA Paper 2003-5355, Aug. 2003.

[2] Hablani, H. B., "Imaging Sensor Pointing and Tracking Controller Insensitive to Gyros and Star Trackers Misalignments," AIAA Paper 2005-5982, 2005.

[3] Markley, F. L., and Reynolds, R. G., "Analytic Steady-State Accuracy of a Spacecraft Attitude Estimator," *Journal of Guidance, Control, and Dynamics*, Vol. 23, No. 6, 2000, pp. 1065–1067.

[4] Anderson, B. D. O., and Moore, J. B., *Optimal Filtering*, Prentice–Hall, Upper Saddle River, NJ, 1979, Secs. 5.4–5.5, pp. 105–121.

[5] Sandhu, G. S., "Rigid Body Mode Pointing Accuracy and Stability Criteria for an Orbiting Spacecraft," *Journal of Spacecraft and Rockets*, Vol. 11, No. 8, 1974, pp. 599–601.

[6] Grewal, M. S., and Andrews, A. P., *Kalman Filtering: Theory and Practice*, Prentice–Hall, Upper Saddle River, NJ, 1993, Sec. 3.4, 9, pp. 71–72.

[7] Elishakoff, I., *Probabilistic Methods in the Theory of Structures*, Wiley, New York, 1983, Appendix C, p. 472.

[8] Franklin, G. F., Powell, J. D., and Workman, M., *Digital Control of Dynamic Systems*, 3rd ed., Addison Wesley, Reading MA, 1998, pp. 433–434.

[9] Bar-Shalom, Y., Rong Li, X., and Kirubarajan, T., *Estimation with Applications to Tracking and Navigation*, Wiley, New York, 2001, Sec. 10.3, p. 389; Chap. 11; Sec. 6.2.2; Sec. 4.3.4; Chap. 12.

[10] Pittelkau, M. E., "Kalman Filtering for Spacecraft System Alignment Calibration," *Journal of Guidance, Control, and Dynamics*, Vol. 24, No. 6, 2001, pp. 1187–1195.

[11] Gelb, A. (ed.), *Applied Optimal Estimation*, MIT Press, Cambridge, MA, 1974, Chap. 9.

[12] Rogers, R. M., *Applied Mathematics in Integrated Navigation Systems*, 2nd ed., AIAA Education Series, AIAA, Reston, VA, 2003, p. 205.

[13] Van der Ha, J., and Mugellesi, R., "Analytical Models for Relative Motion Under Constant Thrust," *Journal of Guidance, Control, and Dynamics*, Vol. 13, No. 4, 1990, pp. 644–650.

[14] Markley, F. L., "Fast Quaternion Attitude Estimation from Two Vector Measurements," *Journal of Guidance, Control, and Dynamics*, Vol. 25, No. 2, 2002, pp. 411–414.

[15] Hablani, H. B., Tapper, M. L., and Dana-Bashian, D. J., "Guidance Algorithms for Autonomous Rendezvous of Spacecraft in Circular Orbits," *Journal of Guidance, Control, and Dynamics*, Vol. 25, No. 3, May–June 2002, pp. 553–562.

[16] Montenbruck, O., and Gill, E., *Satellite Orbits: Models, Methods, and Applications*, Springer, New York, 2000, p. 205, Chap. 6, Sec. 9.2.